iScience

CellPress
OPEN ACCESS

Article

Syndecan-1 Stimulates Adult Neurogenesis in the Mouse Ventricular-Subventricular Zone after Injury

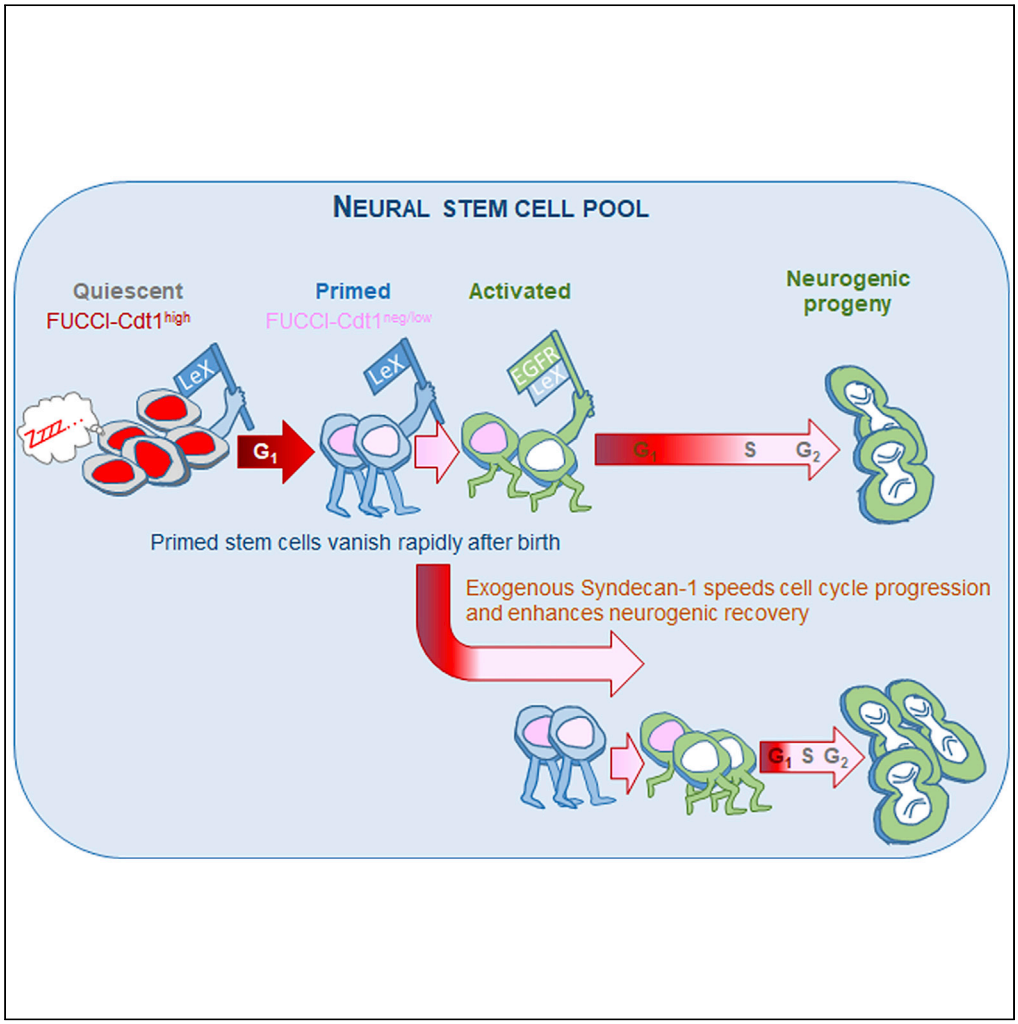

Marc-André Mouthon, Lise Morizur, Léa Dutour, Donovan Pineau, Thierry Kortulewski, François D. Boussin

marc-andre.mouthon@cea.fr (M.-A.M.)
francois.boussin@cea.fr (F.D.B.)

HIGHLIGHTS

A subpopulation of quiescent NSCs are primed to enter cell cycle

The content of primed quiescent NSCs decreases rapidly with age

Syndecan-1 favors cell cycle progression of NSCs *in vitro* and *in vivo*

Mouthon et al., iScience *23*, 101784
December 18, 2020
https://doi.org/10.1016/j.isci.2020.101784

iScience

CellPress
OPEN ACCESS

Article

Syndecan-1 Stimulates Adult Neurogenesis in the Mouse Ventricular-Subventricular Zone after Injury

Marc-André Mouthon,[1,2,*] Lise Morizur,[1] Léa Dutour,[1] Donovan Pineau,[1] Thierry Kortulewski,[1] and François D. Boussin[1,*]

SUMMARY

The production of neurons from neural stem cells (NSCs) persists throughout life in the mouse ventricular-subventricular zone (V-SVZ). We have previously reported that NSCs from adult V-SVZ are contained in cell populations expressing the carbohydrate SSEA-1/LeX, which exhibit either characteristics of quiescent NSCs (qNSCs) or of actively dividing NSCs (aNSCs) based on the absence or the presence of EGF-receptor, respectively. Using the fluorescence ubiquitination cell cycle indicator-Cdt1 transgenic mice to mark cells in G_0/G_1 phase of the cell cycle, we uncovered a subpopulation of qNSCs which were primed to enter the cell cycle *in vitro*. Besides, we found that treatment with Syndecan-1, a heparan sulfate proteoglycan involved in NSC proliferation, hastened the division of qNSCs and increased proliferation of aNSCs shortening their G_1 phase *in vitro*. Furthermore, administration of Syndecan-1 ameliorated the recovery of neurogenic populations in the V-SVZ after radiation-induced injury providing potential cure for neurogenesis decline during brain aging or after injury.

INTRODUCTION

The generation of neurons, astrocytes, and oligodendrocytes persists throughout life in specific regions of the mammalian brain and contributes to neural plasticity through rewiring, refreshing of established networks, and maintenance of cognition (Kempermann et al., 2018). Remarkably, two main regions of the forebrain exhibit germinative potentials, namely the subgranular zone of the dentate gyrus in the hippocampus and the ventricular-subventricular zone (V-SVZ) (Obernier and Alvarez-Buylla, 2019). Adult neurogenesis within the V-SVZ is insured by neural stem cells (NSCs), or type B cells, that enter the cell cycle then successively give rise to transit amplifying cells (type C) and neuroblasts (type A) which differentiate into neurons once they have reached the olfactory bulbs (Obernier and Alvarez-Buylla, 2019).

In the adult brain, NSCs are contained in two populations of quiescent NSCs (qNSCs) and active NSCs (aNSCs) with different cell cycle features (Codega et al., 2014; Daynac et al., 2013). Particularly, owing to their high proliferative capacity, proliferating aNSCs are rapidly eliminated in the V-SVZ after anti-mitotic treatment, whereas qNSCs resist and then re-entering the cell cycle to insure progressive recovery of neurogenesis (Codega et al., 2014; Daynac et al., 2013; Llorens-Bobadilla et al., 2015; Mich et al., 2014). The majority of adult NSCs are produced during embryonic days (E13.5 - E15.5) in the mouse and remain largely quiescent until they become reactivated postnatally contributing to neurogenesis (Fuentealba et al., 2015; Furutachi et al., 2015).

Defects of neurogenesis occur during aging and most studies agree that it is related to a progressive reduction in the number of proliferating cells in the V-SVZ (Blackmore et al., 2009; Enwere et al., 2004; Maslov et al., 2004; Tropepe et al., 1997). Cell cycle alterations of NSCs or decline in their number explained the age-related neurogenesis decline and are already visible at 6 months in the adult mouse (Bouab et al., 2011; Daynac et al., 2014, 2016a; Luo et al., 2008). Several factors from the neurogenic niche, including inflammatory factors, have been shown to reduce neurogenesis during aging by altering the cell cycle of NSCs (Daynac et al., 2014; Kalamakis et al., 2019; Pineda et al., 2013; Silva-Vargas et al., 2016). Quiescence of NSCs has also been shown to be triggered by Wnt antagonist in the aging brain (Kalamakis et al., 2019).

[1]Université de Paris and Université Paris-Saclay, Inserm, LRP/iRCM/IBFJ CEA, UMR Stabilité Génétique Cellules Souches et Radiations, 92265 Fontenay-aux-Roses, France

[2]Lead Contact

*Correspondence: marc-andre.mouthon@cea.fr (M.-A.M.), francois.boussin@cea.fr (F.D.B.)

https://doi.org/10.1016/j.isci.2020.101784

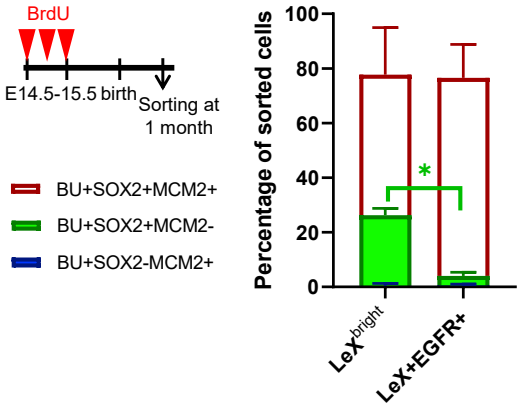

Figure 1. Young Adult LeX^{bright} qNSCs Are Produced during Embryogenesis

BrdU was given to pregnant mice (from E14.5 to E15.5), and then LeX + EGFR + aNSCs and LeX^{bright} qNSCs were sorted using a combination of CD24/LeX/EGFR membrane markers one month after birth and BrdU incorporation was quantified together with SOX2 and MCM2. Data are represented as median ± interquartile range from replicate experiments (n = 4) with 2–4 mice per group. See also Figure S1. *P < 0.05.

Syndecan-1 (SDC1, CD138) is a cell surface heparan sulfate proteoglycan that has been reported to modulate neural progenitor proliferation during embryogenesis through Wnt signaling pathways (Wang et al., 2012). Recently, we reported on a different expression pattern of SDC1 between qNSCs and aNSCs and demonstrated its role in the proliferation of aNSCs in the postnatal V-SVZ (Morizur et al., 2018).

Here, we examined in more detail alterations during aging of NSC proliferation from postnatal V-SVZ in mice particularly with regards to capacity of qNSCs to enter cell cycle and the effects of exogenous SDC1 on NSC proliferation.

RESULTS

LeX^{bright} qNSCs Are Produced during Embryogenesis

We previously reported on an FACS strategy to sort LeX^{bright} qNSCs and LeX + EGFR + aNSCs from the adult mouse and early postnatal V-SVZ based on the absence of CD24 expression and the differential expression of the membrane markers EGFR and LeX (Daynac et al., 2013, 2015; Morizur et al., 2018). These LeX^{bright} qNSCs and LeX + EGFR + aNSCs exhibit strikingly similar molecular profiles to that obtained by other strategies, including anti-GLAST antibody, and/or transgenic GFAP:GFP mice in adult V-SVZ (Beckervordersandforth et al., 2010; Codega et al., 2014; Llorens-Bobadilla et al., 2015; Mich et al., 2014).

Adult NSCs have been reported to be produced during mid-embryonic development in the mouse and remain largely quiescent until they become reactivated postnatally (Fuentealba et al., 2015; Furutachi et al., 2015). Therefore, to mark qNSCs generated during embryogenesis, BrdU was administrated to pregnant mice from E14.5 to E15.5. qNSCs that underwent rare divisions, if any, were characterized by BrdU-label retention in postnatal brains (one month after birth). Immunostaining of SOX2 was used to confirm NSC identity and labeling of the G1 phase cell cycle marker MCM2 was used to detect both slowly and rapidly cycling NSCs (Maslov et al., 2004). LeX^{bright} qNSCs and LeX + EGFR + aNSCs were sorted from V-SVZ one month after birth. Although they are actively dividing cells *in vivo* (Morizur et al., 2018), LeX + EGFR + aNSCs were in great majority (72%) BrdU/SOX2/MCM2-triple positive and had a BrdU staining less intense in comparision to LeX^{bright} qNSCs, suggesting that they derived from the later with few divisions (Figures 1 and S1). On the other hand, the majority of LeX^{bright} cells (82%) was positive for BrdU confirming their embryonic origin (Figures 1 and S1). Moreover, 56.8% of LeX^{bright} cells were BrdU/SOX2/MCM2-triple positive cells, i.e. very long-term qNSCs, whereas 25% were BrdU+/SOX2+/MCM2-negative i.e. likely differentiated astrocytes.

These data confirmed thus that the LeX^{bright} qNSCs from the postnatal brain are produced during embryogenesis similarly as previously reported by others using *in vivo* approaches (Fuentealba et al., 2015; Furutachi et al., 2015).

The Subpopulation of Primed LeX^{bright} qNSCs Able to Enter the Cell Cycle Rapidly Decreases with Age

Many structural and cellular modifications of the V-SVZ progressively occur during the early postnatal development and later in the adult brain, but data on the cell cycle status of NSCs associated with these changes are still incompletely documented. qNSCs and aNSCs identity in early postnatal V-SVZ was

confirmed with GFAP expression, a marker of adult-type B/NSCs (Doetsch et al., 1999) and MCM2 expression. LeX^{bright} and LeX + EGFR + cells were sorted from early postnatal V-SVZ (10 days). Both LeX^{bright} qNSCs and LeX + EGFR + aNSCs expressed GFAP (Figure S2). MCM2, which is expressed in actively dividing cells and slowly cycling NSCs (Maslov et al., 2004), was detected on 65% of LeX + EGFR + aNSCs but also 25% of LeX^{bright} qNSCs (Figure S2C), confirming that a part of qNSCs were primed to enter cell cycle at this developmental stage.

To further examine cell cycle alterations of NSC populations from early postnatal pups to aged mice, we used fluorescence ubiquitination cell cycle indicator (FUCCI) Cdt1-red transgenic mice. FUCCI-Cdt1 system allows the visualization of cells in G1 with the presence of a G1-specific red-Cdt1 reporter (FUCCI^{pos}), while it is absent in cells during the S/G2/M phases (FUCCI^{neg}) (Sakaue-Sawano et al., 2008). In addition, FUCCI^{high} allows the identification of cells that have exited the cell cycle (G0 cells) (Daynac et al., 2014; Roccio et al., 2013).

At each developmental stage, most LeX + EGFR + aNSCs were in G1 (FUCCI^{low}) and in S/G2/M phases (FUCCI^{neg}), and fewer had exited cell cycle (FUCCI^{high}) according to their active proliferating status (Figure 2A and Table S1). Interestingly, we found higher proportions of aNSCs in G0 (FUCCI^{high}) in the early postnatal brains than in the adult brains, which is reminiscent of an extensive differentiation associated with the brain development after birth. Moreover, the ratio of cells in G1 (FUCCI^{low}) over S/G2/M phases (FUCCI^{neg}) was higher in the early postnatal brain than in adult brain indicating a longer G1 phase.

On the contrary, a large proportion of LeX^{bright} qNSCs had exited the cell cycle (FUCCI^{high}) at all developmental stages in accordance with their quiescent status (Figure 2B). Nonetheless, we found between 21.6% and 33.2% of LeX^{bright} qNSCs that were either in G1 (FUCCI^{low}) or in S/G2/M (FUCCI^{neg}), whatever the developmental stage, highlighting that a significant and stable fraction of qNSCs are primed to enter cell cycle in the V-SVZ from both early postnatal and adult mouse brain. Nonetheless, a significant fraction of LeX^{bright} qNSCs were in G1 (FUCCI^{low}), but few of them were actively cycling (FUCCI^{neg}) (Figure 2B). Markedly, the percentage of LeX^{bright} qNSCs in S/G2/M (FUCCI^{neg}) dropped in the young adult mice (Figure 2B).

We then compared the capacities of LeX^{bright} qNSCs and LeX + EGFR + aNSCs sorted from PN10 and young adult V-SVZ to proliferate and to form neurospheres, which are floating clones initiated by actively dividing NSCs (Pastrana et al., 2011). LeX + EGFR + aNSCs had a similar clonogenic capacity in early postnatal and adult brains (Figure 2C). In addition, LeX + EGFR + subpopulations were sorted according to FUCCI (FUCCI^{low}: G1 and FUCCI^{neg}: S/G2/M) but presented no difference of clonogenic capacity at both ages (Figure S3). Besides, accordingly with their quiescent status, LeX^{bright} qNSCs from neonatal brain had a 15.5 times lower clonogenic capacity than their activated LeX + EGFR + aNSCs counterparts (Figure 2C). Clonogenic capacity of LeX^{bright} qNSCs was further decreased by more than 100-fold in the adult brain. This decrease in clonogenic capacity appeared to reflect the disappearing of clonogenic LeX^{brigh} cells rather than their positioning within cell cycle since LeX^{bright} FUCCI^{low} and FUCCI^{neg} had similar clonogenicity (Figure S3). This extremely low clonogenic capacity of LeX^{bright} qNSCs in young adult V-SVZ contrasted with their MCM2 expression (Figure 1), suggesting that most primed LeX^{bright} qNSCs are not fully activated to generate clones.

Our data revealed an early cell cycle alteration of LeX + EGFR + aNSCs in early postnatal pups most probably coinciding with differentiation during development. Additionally, some LeX^{bright} qNSCs entered the cell cycle in the early postnatal, whereas they were blocked in G1 in the young adult mice.

A Subpopulation of LeX^{bright} FUCCI$^{neg/low}$ qNSCs Maintains the Capacity to Enter Proliferation in the Young Adult V-SVZ

LeX^{bright} qNSC and LeX + EGFR + aNSC populations were sorted from the V-SVZ of young adult mice and then plated in enriched NSC medium supplemented with BrdU (10 μM) to challenge their proliferation capacities. After 72hr, the great majority of LeX + EGFR + aNSCs (84.2 ± 3.4%) had incorporated BrdU and exhibited an active protein synthesis activity as seen with phosphorylation of S6 ribosomal protein (69.8 ± 3.4%) (Figures 3A and 3B). By contrast, only 27.2 ± 9.8% of LeX^{bright} qNSCs had incorporated BrdU, and few of them (3.1 ± 1.6%) were positive for phosphoS6 ribosomal protein (Figures 3A and 3B). Both BrdU incorporation and pS6 suggested that a subpopulation of qNSCs was primed to enter cell cycle as previously reported (Codega et al., 2014; Llorens-Bobadilla et al., 2015).

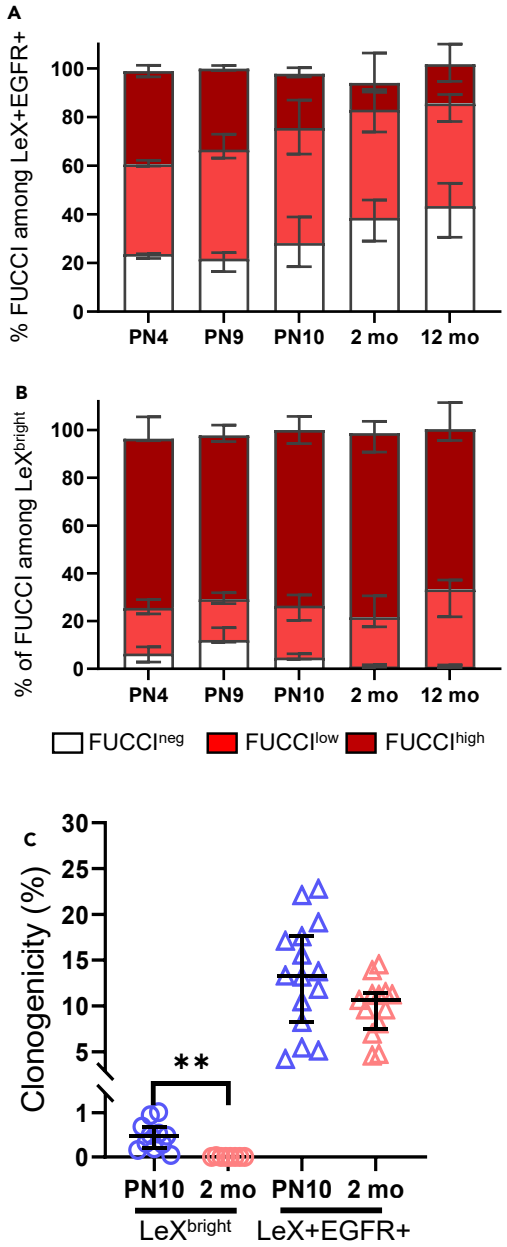

Figure 2. Cell Cycle Status and Clonogenic Capacities of LeX^{bright} qNSCs and LeX + EGFR + aNSCs in the Postnatal V-SVZ

(A and B) FUCCI fluorescence was determined by flow cytometry in V-SVZ at various postnatal ages. The percentage of different FUCCI populations (FUCCI^{high}: G0; FUCCI^{low}: G1 and FUCCI^{neg}: S/G2/M) was represented among (A) LeX + EGFR + aNSCs and (B) LeX^{bright} qNSCs.

(C) The formation of neurospheres, i.e. clonogenic capacity, was determined 7 days after sorting LeX^{bright} qNSCs and LeX + EGFR + aNSCs from 10 days- to 2 months-old V-SVZ. Data were compared using non-parametric Kruskal-Wallis and Dunn's multicomparison tests and given in Table S1. Data are represented as median ± interquartile. Each dot in C represents individual experiment. See also Table S1 and Figure S3. **P < 0.005.

To further explore the capacity of these LeX^{bright} qNSCs to re-enter into the cell cycle, we prospectively sorted them from the young adult FUCCI V-SVZ and challenged their proliferation capacities by *in vitro* time-lapse videomicroscopy.

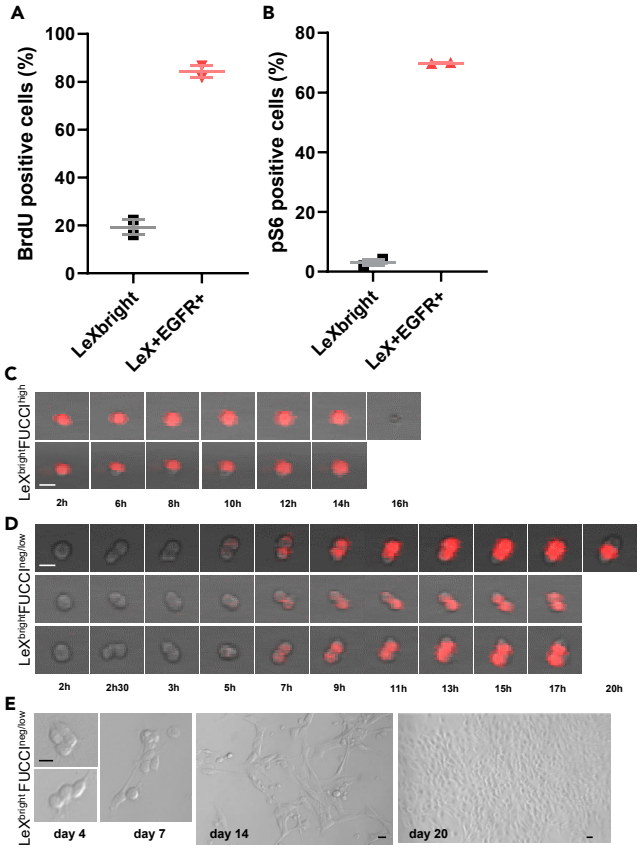

Figure 3. LeX^{bright} FUCCI$^{neg/low}$ qNSCs Divide and Initiate Clones *In Vitro* but FUCCI^{high} NSCs Have Definitively Exited the Cell Cycle

(A and B) LeX^{bright} qNSCs and LeX + EGFR + aNSCs were sorted from young adult mouse V-SVZ and then cultured in the presence of BrdU for 72hr *in vitro*.

(A) Percentages of BrdU incorporation and (B) pS6-positive cells were quantified in LeX^{bright} qNSCs and LeX + EGFR + aNSCs from replicate experiments with a total number of 66–144 cells.

(C–E) LeX^{bright} cells were sorted from young adult V-SVZ according to their FUCCI-Cdt1 fluorescence intensity and were followed by time-lapse videomicroscopy. (C) LeX^{bright} FUCCI^{high} cells never divide but (D) the LeX^{bright} FUCCI$^{neg/low}$ population showed divisions. (E) Thereafter, formation of clones was rarely observed in the LeX^{bright} FUCCI$^{neg/low}$ qNSCs. Scale bars = 10μm.

On one hand, FUCCI^{high} cells representing the majority of LeX^{bright} population (interquartile range [67.9%–79.2%]) had apparently exited the cell cycle and presented a bright red fluorescence *in vitro,* which eventually disappeared when cells died but they never divided (Figure 3C). On the other hand, 20% of the FUCCI$^{neg/low}$ population of LeX^{bright} qNSCs, encompassing G1 and scarce S/G2/M cells, had divided during the first 26hr (Figure 3D). Then FUCCI fluorescence showed an increase which became high in some LeX^{bright} qNSCs. Thereafter, FUCCI$^{neg/low}$ LeX^{bright} qNSCs very scarcely generated clones that grew slowly and ultimately gave rise to larger clones (Figure 3E).

Altogether, these data show that some of the LeX^{bright} qNSCs were primed to re-enter cell cycle *in vitro* and were contained within the FUCCI$^{neg/low}$ population.

Recombinant Syndecan-1 Shortens Cell Cycle Progression *In Vitro*

We have shown that SDC1 is highly expressed in proliferating LeX + EGFR + aNSCs from adult mice while it is found at low levels in LeX^{bright} qNSCs (Morizur et al., 2018). Here, we reported that SDC1 mRNAs were expressed at a similar level in LeX + EGFR + aNSCs from neonatal and adult mice (Figure S4). Although the expression of SDC1 mRNAs was low in LeX^{bright} qNSCs from neonates, it showed

a further decline in adult mice (Figure S4) coinciding with the drop in clonogenic capacities. We have previously reported that SDC1 knockdown reduces proliferation of LeX + EGFR + aNSCs (Morizur et al., 2018). Likewise, addition of chondroitinase ABC (50 and 100 U/mL) which degrades chondroitin sulfate proteoglycans, including SDC1, reduced the formation of neurospheres initiated by LeX + EGFR + aNSCs (data not shown). Conversely, deglycanation of SDC1 with heparanase (4 ng/mL) which transforms SDC1 into a highly selective surface-binding protein (Ma et al., 2006) increased BrdU incorporation in proliferating NSCs (data not shown).

Therefore, we tested the effects of exogenous recombinant SDC1 (recSDC1) on proliferation of NSCs freshly sorted from young adult mice. Two days after plating, LeX + EGFR + aNSCs gave rise to small colonies containing 4-6 cells in control conditions and 4-8 cells in the presence of 2.5μg/ml of recSDC1. This increase was further observed on neurosphere size at 6 days in the presence of 2.5 μg/mL of rec SDC1 (Figure 4A). This increase in neurosphere size inversely mirrored the data we previously reported after silencing SDC1 (Morizur et al., 2018). Besides, the clonogenic efficacy of LeX + EGFR + aNSCs appeared to be almost significantly increased in the presence of recSDC1 (Figure 4B).

We thus investigated the effects of recSDC1on cell cycle length of LeX + EGFR + aNSCs by time-lapse videomicroscopy using FUCCI mice. Interestingly, the time for the first division of LeX + EGFR + aNSCs from neonates was significantly shortened in the presence of 2.5μg/ml of recSDC1 in comparison to control (Figure 4C). A similar shortening was observed in young adult V-SVZ (Figure S5). The length of the G1 phase was measured for the subsequent cycle taking advantage of the FUCCI-Cdt1 fluorescence. A significant shortening of the G1 phase was observed in LeX + EGFR + aNSCs (Figure 4D). We then investigated the effects of recSDC1 on LeX^{bright} $FUCCI^{neg/low}$ qNSCs, i.e. primed qNSCs. The percentage of dividing LeX^{bright} $FUCCI^{neg/low}$ appeared not significantly increased in the presence of SDC1 (Figure 4E). Strikingly, the time for the first division of LeX^{bright} $FUCCI^{neg/low}$ qNSCs was significantly shortened in the presence of 2.5μg/ml of recSDC1 (7h36) in comparison to control (9h12) (Figure 4F). However, LeX^{bright} $FUCCI^{neg/low}$ cells remained FUCCI-Cdt1 positive at the end of the videomicroscopy (28-30hr) and did not re-enter in another division cycle even in the presence of recSDC1. By contrast, $FUCCI^{high}$ LeX^{bright} cells did not divide even in the presence of SDC1 (data not shown). Strikingly, 25% (first interquartile) of LeX^{bright} $FUCCI^{neg/low}$ and LeX + EGFR + NSCs exposed to SDC1 had divided before 5h and 7h for adults and neonates, respectively, suggesting that numerous aNSCs and qNSCs might be blocked in G_2.

Altogether, our data show that SDC1 favored cell cycle progression of primed qNSCs and aNSCs.

Recombinant Syndecan-1 Accelerates Recovery of Neurogenic Populations *In Vivo*

Subsequently, we addressed the capacity of recSDC1 to ameliorate V-SVZ recovery *in vivo* after brain irradiation in young adult FUCCI-Cdt1 transgenic mice. After such radiation-induced injury, highly proliferating cells, including LeX + EGFR + aNSCs, are rapidly eliminated, whereas LeX^{bright} qNSCs are radioresistant and enter cell cycle 48hr after exposure, which is followed by the progressive recolonization of the V-SVZ by LeX + EGFR + aNSCs, EGFR + progenitors and CD24 + EGFR + young neuroblasts (Daynac et al., 2013). Collection of V-SVZ cells from young adult FUCCI-Cdt1 mice 48hr after irradiation demonstrated the elimination of the majority of LeX + EGFR + aNSCs, EGFR+ and CD24 + EGFR + cells while leaving a significant amount of LeX^{bright} $FUCCI^{neg/low}$ qNSCs, i.e. progressing throughout the cell cycle (Figure 5). Recombinant SDC1 was administrated intraventricularly while mice received BrdU through systemic route and recovery of neurogenic populations was analyzed three days later. The absolute counts of the neurogenic populations revealed that recSDC1 favored primarily the recovery of EGFR+ and CD24 + EGFR + cells (Figures 5 and S6A). Interestingly, the increase in these EGFR+ and CD24 + EGFR + neurogenic populations with recSDC1 was observed in the $FUCCI^{low}$ and $FUCCI^{neg}$ cycling populations (Figures 5C and 5D) and was associated with BrdU incorporation, i.e. proliferation (Figure S6B). On the other hand, the presence of recSDC1 did not significantly improve the recovery of LeX^{bright} qNSCs and LeX + EGFR + aNSCs (Figures 5A and 5B) while BrdU incorporation indicated their proliferation (Figure S6B). Part of the LeX + EGFR + aNSCs had even exited cell cycle, i.e. $FUCCI^{high}$ (Figure 2B). Nevertheless, this would be expected from asymmetric division of NSCs and their subsequent loss instead of EGFR+ and CD24 + EGFR + which undergo symmetric division.

These data show that SDC1 favored recovery of neurogenic populations in the V-SVZ after injury.

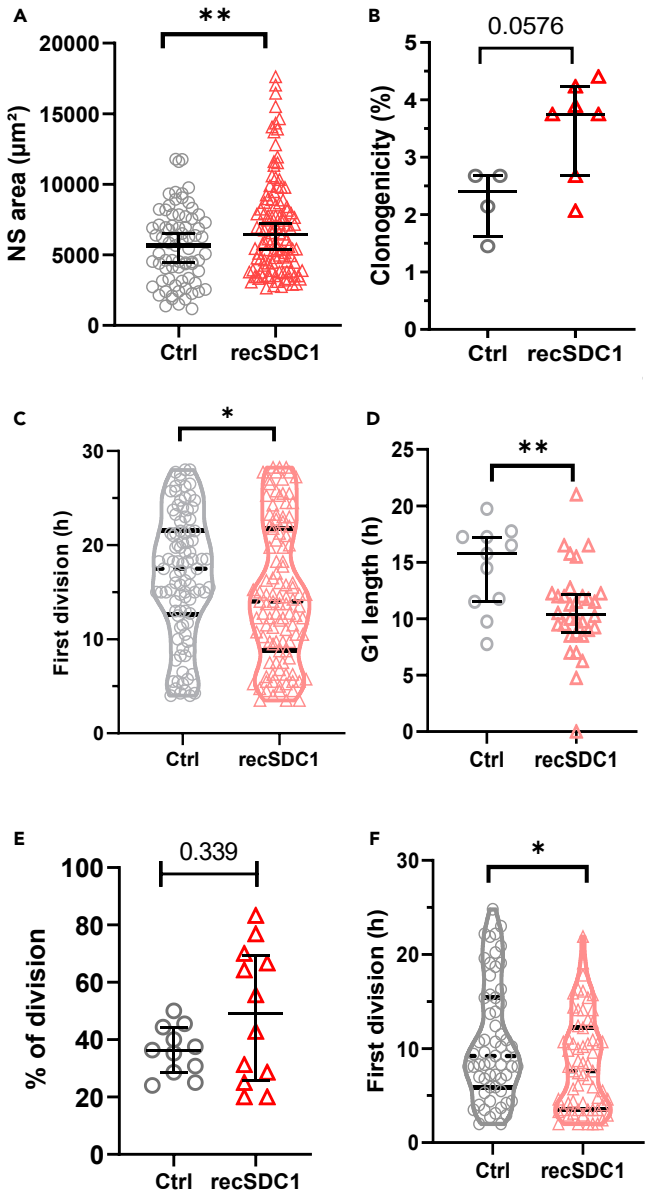

Figure 4. Recombinant SDC1 Increases the Neurosphere Size of aNSCs and Hastens the Division of aNSCs and qNSCs

(A and B) LeX + EGFR + aNSCs were sorted from young adult V-SVZ. After 6 days in culture of LeX + EGFR + aNSCs in the absence, or the presence, of 2.5µg/ml recSDC1: (A) the neurosphere area (μm^2) and (B) clonogenic capacities were determined.

(C and D) LeX + EGFR + aNSCs were sorted from FUCCI neonates and were followed by time-lapse for 26-30hr in the absence, or the presence, of 2.5µg/ml recSDC1, then (C) the time for the first division and (D) the length of the subsequent G_1 were recorded.

(E and F) LeX^{bright} $FUCCI^{neg/low}$ qNSCs were sorted from adult FUCCI mice, then (E) the percentage of dividing cells/field and (F) the time for the first division were recorded. Data are represented as the median ± interquartile range of replicate experiments with 2–4 mice per group. See also Figure S5. *P < 0.05; **P < 0.005.

DISCUSSION

Different FACS strategies have been reported for the isolation of qNSCs and aNSCs (Beckervordersandforth et al., 2010; Codega et al., 2014; Daynac et al., 2013; Llorens-Bobadilla et al., 2015; Mich et al., 2014). Briefly, anti-GLAST or anti-LeX antibodies or GFAP:GFP are used as NSC markers in combination

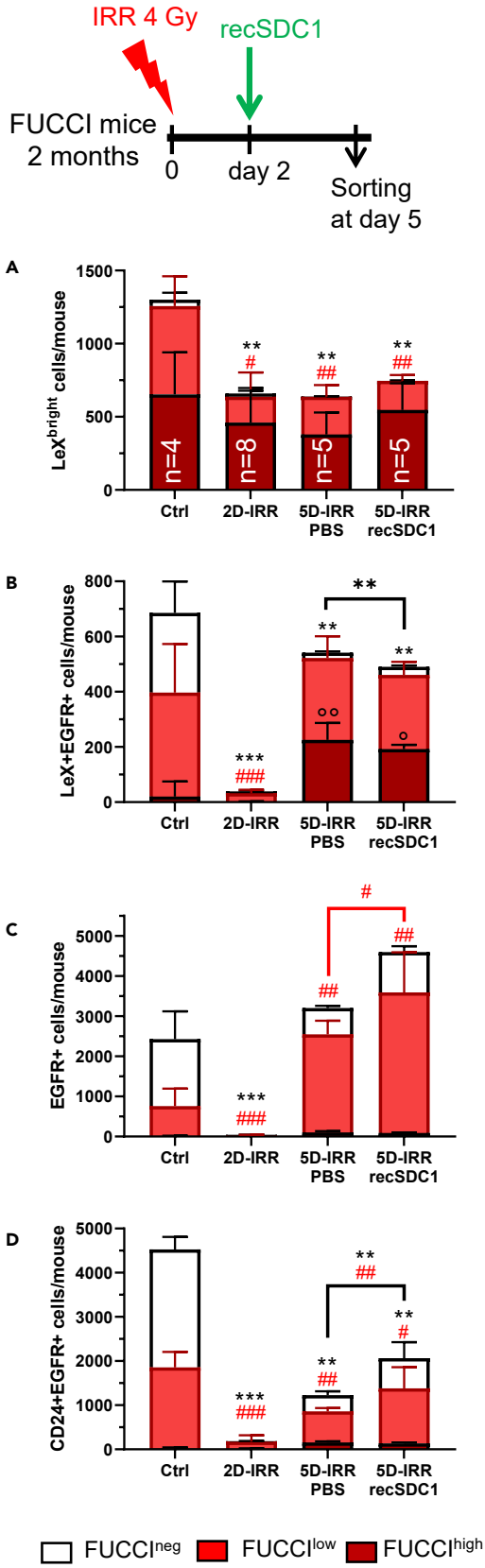
IRR 4 Gy
recSDC1
FUCCI mice
2 months
0
day 2
Sorting
at day 5
A
LeX^bright cells/mouse
1500
1000
500
0
n=4
n=8
n=5
n=5
Ctrl
2D-IRR
5D-IRR PBS
5D-IRR recSDC1
B
LeX+EGFR+ cells/mouse
800
600
400
200
0
C
EGFR+ cells/mouse
5000
4000
3000
2000
1000
0
D
CD24+EGFR+ cells/mouse
FUCCI^neg
FUCCI^low
FUCCI^high

Figure 5. Exogenous SDC1 Favors Recovery of Neurogenic Populations after Radiation-Induced V-SVZ Injury

For a Figure360 author presentation of this figure, see https://doi.org/10.1016/j.isci.2020.101784. Figure360▷

(A–D) Two-months-old adult FUCCI-Cdt1 mice were irradiated (4 Gy/head only) and received recSDC1 intraventricularly. The absolute numbers of (A) LeX^{bright} qNSCs, (B) LeX + EGFR + aNSCs, (C) EGFR + progenitors, and (D) CD24 + EGFR + proliferating neuroblasts and FUCCI fluorescence were determined by flow cytometry within FUCCI subpopulations (FUCCI^{high}: G0; FUCCI^{low}: G1 and FUCCI^{neg}: S/G2/M). Data are represented as median ± interquartile range. Each plot represents an individual mouse (the number of mice is indicated within bars). Data were compared using non-parametric Kruskal-Wallis and Dunn's multicomparison tests. Comparisons with the Ctrl group are given upper the boxes and comparisons between PBS and recSDC1 over the brackets (° for FUCCI^{high}; # for FUCCI^{low} and * for FUCCI^{neg}). See also Figure S6.

with other markers. Interestingly, qNSCs and aNSCs obtained from these different methods have strikingly similar molecular profiles. Particularly, qNSCs being characterized by the expression of several genes as Prom1, Aldh1l1, Gjb6, CD9, Sox9, Id2 and Id3, whereas aNSCs expressing high level of Ascl1, Egr1, Fos, Sox4, and Sox11 (Beckervordersandforth et al., 2010; Codega et al., 2014; Daynac et al., 2013; Llorens-Bobadilla et al., 2015; Mich et al., 2014). In addition, we have shown that LeX^{bright} qNSCs are produced during embryogenesis similarly as previously reported by for type B/NSCs *in vivo* (Fuentealba et al., 2015; Furutachi et al., 2015).

A pool of NSCs remains largely dormant until qNSCs become reactivated postnatally contributing to neurogenesis for brain homeostasis or repair after injury (Daynac et al., 2013). Using the FUCCI-Cdt1 system, we reported, here, on the prospective isolation of primed qNSC. Interestingly, we demonstrate that the capacity of qNSCs to enter cell cycle declines as early as in the young adult mouse brain. However, we have shown that cell cycle progression of LeX^{bright} qNSCs is favored by addition of exogenous SDC1.

Adult neurogenesis declines with aging due to the depletion and functional impairment of neural stem/progenitor cells. In this context, previous reports have indicated that the number of NSCs in the mouse V-SVZ declines by mid-age (10-12 months), with an additional reduction in older mice (22 months) reviewed in (Lupo et al., 2019). While prior studies have demonstrated a reduction of NSC content and have noted a paradoxical increase in the NSC division rate in old animals (Luo et al., 2008; Shook et al., 2012), we observed a decline in cell cycle activity of aNSCs at mid-age (6-12 months) but with stable contents (Daynac et al., 2014, 2016a). These seemingly divergent data are reconciled by the fluctuation of NSC proliferation with a decline between 2 and 18 months, and then unexpectedly a reversal faster cell cycle at 22 months (Apostolopoulou et al., 2017). On the other hand, increasing NSC quiescence is predicted to contribute to the age-related decline of neurogenesis (Bast et al., 2018; Kalamakis et al., 2019). NSCs begin undergoing quiescence-associated changes at mid-adulthood in the mouse V-SVZ (Bouab et al., 2011).

Using various approaches based on FUCCI-Cdt1, BrdU incorporation, clonogenicity, which showed consistency, we have shown that proliferation capacities of NSCs decreased early in the postnatal V-SVZ. Particularly, aNSCs showed a G1 lengthening in the early postnatal V-SVZ associated with cell cycle exit which is in accordance with differentiation during brain development (Salomoni and Calegari, 2010). Grippingly, we have identified a population among LeX^{bright} qNSCs that are characterized by a low FUCCI-Cdt1 fluorescence which are primed to enter the cell cycle. The population of LeX^{bright} is able to re-entry into cell cycle after V-SVZ irradiation accordingly to what was previously reported (Daynac et al., 2013) and similarly to what was shown for other brain injuries (Codega et al., 2014; Llorens-Bobadilla et al., 2015; Mich et al., 2014). Noticeably, we have shown a drop of primed LeX^{bright} FUCCI^{neg} qNSCs entering the cell cycle in the young adult which was associated to the decline in their clonogenic capacities. Although expressing a significant level of SOX2 and MCM2, marking slow dividing NSC (Maslov et al., 2004), LeX^{bright} cells divided once, then stopped in G_1 but very scarcely formed neurospheres in neonates and even more rarely when isolated from young adults. This might indicate that experimental conditions are not adequate for NSC proliferation *in vitro* and/or that high LeX expression interfered with NSC proliferation as previously reported (Luque-Molina et al., 2017). These early events are reminiscent to the human V-SVZ which shows a drop in neurogenesis several months after birth (Sanai et al., 2011). This continuum of NSC proliferation decline starting at birth is linked to postnatal brain development. Also, this suggests that qNSCs are recruited, through their activation, early during the postnatal brain development. Therefore, NSC quiescence appears as a programmed developmental process and a consequence of molecular aging processes.

Loss of the ability of qNSCs to activate and/or proliferation defect during aging are related to alterations of transcriptomic or lysosomal activities (Leeman et al., 2018; Lupo et al., 2018). Raise in inflammatory factors within the neurogenic niche has also been shown to reduce neurogenesis by altering the cell cycle or quiescence of NSCs during aging (Daynac et al., 2014, 2016a; Engler et al., 2018; Kalamakis et al., 2019; Pineda et al., 2013; Silva-Vargas et al., 2016). Several signaling pathways such as WNT or Sonic Hedgehog have been involved in the regulation of NSC quiescence and proliferation (Chavali et al., 2018; Daynac et al., 2016b). Interestingly, activation of LeX^{bright} qNSCs after radio-induced injury was associated with the up-regulation of several genes belonging to WNT signaling (Table S2). Conversely, the niche-derived WNT antagonist sFRP5 has been shown to induce quiescence in the aging brain (Kalamakis et al., 2019).

SDC1 plays a role in NSC proliferation during embryogenesis and in postnatal NSCs (Morizur et al., 2018; Wang et al., 2012). SDC1 regulates proliferation in part by modulating the ability of neural progenitors to respond to WNT ligands (Wang et al., 2012). Here, we have shown that addition of exogenous SDC1 favors proliferation of aNSCs *in vitro* through the reduction of the G1 phase. Morever, exogenous SDC1 hastened the time for the first division of primed qNSCs. Interestingly, numerous NSCs divided early after exogenous SDC1 treatment suggesting that they are paused in G_2, as reported in the drosophila (Otsuki and Brand, 2018). Whether these proliferation effects involved WNT signaling needs to be further investigated. Grippingly, exogenous SDC1 also demonstrated *in vivo* activity by favoring recovery of neurogenic populations after V-SVZ injury. Therefore, SDC1 might be used to counteract brain injury. If validated in older animals, administration of SDC1, or of an agonist, might provide the means to control the proliferation of NSCs and to counteract the neurogenesis decline during aging which is still a major concern.

Limitations of the Study

This study has some limitations that should be kept in mind when interpreting the relevance of the findings to regeneration of neurons. Primed LeX^{bright} qNSCs were able to make only a single division suggesting that unknown factor(s) are further required to insure subsequent divisions. Nevertheless, molecular characterization of this rare population might be helpful to identify such factor(s). The administration of recombinant Syndecan-1 ameliorated the recovery of neurogenic populations *in vivo*, but the target cells have to be further characterized. In addition, the production of neurons and their functionality remain to be analyzed. Finally, the transfer to clinic has to take into account that Syndecan-1 might be hijacked by cancer cells to proliferate.

Resource Availability

Lead Contact

Further requests should be directed to and will be fulfilled by the Lead Contact: Marc-André Mouthon (marc-andre.mouthon@cea.fr).

Materials Availability

The study did not generate any unique reagent.

Data and Code Availability

This published article includes all datasets generated or analyzed during this study.

METHODS

All methods can be found in the accompanying Transparent Methods supplemental file.

SUPPLEMENTAL INFORMATION

Supplemental Information can be found online at https://doi.org/10.1016/j.isci.2020.101784.

ACKNOWLEDGMENTS

We are indebted to S. Vincent-Naulleau, V. Neuville, V. Barroca, S. Devanand, and the staff of the animal facilities; to V. Mesnard for irradiation; to J. Baijer and N. Dechamps for cell sorting; and to A. Gouret and A. Leliard for their precious administrative assistance. Flow cytometry and cell sorting were performed at the iRCM Flow Cytometry Shared Resource, established by equipment grants from DIM-Stem-Pôle, INSERM,

Foundation ARC, and CEA. This work was supported by grants from Electricité de France (EDF) and CEA (Segment Radiobiologie).

AUTHORS CONTRIBUTION

M.A.M: conception and supervision, collection and/or assembly of data, data analysis, interpretation and manuscript writing. L.M: conception and design, collection and/or assembly of data, data analysis, interpretation and manuscript writing. L.D., D.P., T.K.: collection and/or assembly of data. F.D.B: funding acquisition, conception, supervision and manuscript writing.

DECLARATION OF INTERESTS

The authors declare no conflict of interest.

Received: April 21, 2020
Revised: September 25, 2020
Accepted: November 5, 2020
Published: December 18, 2020

REFERENCES

Apostolopoulou, M., Kiehl, T.R., Winter, M., Cardenas De La Hoz, E., Boles, N.C., Bjornsson, C.S., Zuloaga, K.L., Goderie, S.K., Wang, Y., Cohen, A.R., and Temple, S. (2017). Non-monotonic changes in progenitor cell behavior and gene expression during aging of the adult V-SVZ neural stem cell niche. Stem Cell Rep. *9*, 1931–1947.

Bast, L., Calzolari, F., Strasser, M.K., Hasenauer, J., Theis, F.J., Ninkovic, J., and Marr, C. (2018). Increasing neural stem cell division asymmetry and quiescence are predicted to contribute to the age-related decline in neurogenesis. Cell Rep. *25*, 3231–3240.e8.

Beckervordersandforth, R., Tripathi, P., Ninkovic, J., Bayam, E., Lepier, A., Stempfhuber, B., Kirchhoff, F., Hirrlinger, J., Haslinger, A., Lie, D.C., et al. (2010). In vivo fate mapping and expression analysis reveals molecular hallmarks of prospectively isolated adult neural stem cells. Cell Stem Cell *7*, 744–758.

Blackmore, D.G., Golmohammadi, M.G., Large, B., Waters, M.J., and Rietze, R.L. (2009). Exercise increases neural stem cell number in a growth hormone-dependent manner, augmenting the regenerative response in aged mice. Stem Cells *27*, 2044–2052.

Bouab, M., Paliouras, G.N., Aumont, A., Forest-Berard, K., and Fernandes, K.J. (2011). Aging of the subventricular zone neural stem cell niche: evidence for quiescence-associated changes between early and mid-adulthood. Neuroscience *173*, 135–149.

Chavali, M., Klingener, M., Kokkosis, A.G., Garkun, Y., Felong, S., Maffei, A., and Aguirre, A. (2018). Non-canonical Wnt signaling regulates neural stem cell quiescence during homeostasis and after demyelination. Nat. Commun. *9*, 36.

Codega, P., Silva-Vargas, V., Paul, A., Maldonado-Soto, A.R., Deleo, A.M., Pastrana, E., and Doetsch, F. (2014). Prospective identification and purification of quiescent adult neural stem cells from their in vivo niche. Neuron *82*, 545–559.

Daynac, M., Chicheportiche, A., Pineda, J.R., Gauthier, L.R., Boussin, F.D., and Mouthon, M.A. (2013). Quiescent neural stem cells exit dormancy upon alteration of GABAAR signaling following radiation damage. Stem Cell Res. *11*, 516–528.

Daynac, M., Morizur, L., Chicheportiche, A., Mouthon, M.A., and Boussin, F.D. (2016a). Age-related neurogenesis decline in the subventricular zone is associated with specific cell cycle regulation changes in activated neural stem cells. Sci. Rep. *6*, 21505.

Daynac, M., Morizur, L., Kortulewski, T., Gauthier, L.R., Ruat, M., Mouthon, M.A., and Boussin, F.D. (2015). Cell sorting of neural stem and progenitor cells from the adult mouse subventricular zone and live-imaging of their cell cycle dynamics. J. Vis. Exp. *14*, 53247.

Daynac, M., Pineda, J.R., Chicheportiche, A., Gauthier, L.R., Morizur, L., Boussin, F.D., and Mouthon, M.A. (2014). TGFbeta lengthens the G1 phase of stem cells in aged mouse brain. Stem Cells *32*, 3257–3265.

Daynac, M., Tirou, L., Faure, H., Mouthon, M.A., Gauthier, L.R., Hahn, H., Boussin, F.D., and Ruat, M. (2016b). Hedgehog controls quiescence and activation of neural stem cells in the adult ventricular-subventricular zone. Stem Cell Rep. *7*, 735–748.

Doetsch, F., Caille, I., Lim, D.A., Garcia-Verdugo, J.M., and Alvarez-Buylla, A. (1999). Subventricular zone astrocytes are neural stem cells in the adult mammalian brain. Cell *97*, 703–716.

Engler, A., Rolando, C., Giachino, C., Saotome, I., Erni, A., Brien, C., Zhang, R., Zimber-Strobl, U., Radtke, F., Artavanis-Tsakonas, S., et al. (2018). Notch2 signaling maintains NSC quiescence in the murine ventricular-subventricular zone. Cell Rep. *22*, 992–1002.

Enwere, E., Shingo, T., Gregg, C., Fujikawa, H., Ohta, S., and Weiss, S. (2004). Aging results in reduced epidermal growth factor receptor signaling, diminished olfactory neurogenesis, and deficits in fine olfactory discrimination. J. Neurosci. *24*, 8354–8365.

Fuentealba, L.C., Rompani, S.B., Parraguez, J.I., Obernier, K., Romero, R., Cepko, C.L., and Alvarez-Buylla, A. (2015). Embryonic origin of postnatal neural stem cells. Cell *161*, 1644–1655.

Furutachi, S., Miya, H., Watanabe, T., Kawai, H., Yamasaki, N., Harada, Y., Imayoshi, I., Nelson, M., Nakayama, K.I., Hirabayashi, Y., and Gotoh, Y. (2015). Slowly dividing neural progenitors are an embryonic origin of adult neural stem cells. Nat. Neurosci. *18*, 657–665.

Kalamakis, G., Brune, D., Ravichandran, S., Bolz, J., Fan, W., Ziebell, F., Stiehl, T., Catala-Martinez, F., Kupke, J., Zhao, S., et al. (2019). Quiescence modulates stem cell maintenance and regenerative capacity in the aging brain. Cell *176*, 1407–1419.e4.

Kempermann, G., Gage, F.H., Aigner, L., Song, H., Curtis, M.A., Thuret, S., Kuhn, H.G., Jessberger, S., Frankland, P.W., Cameron, H.A., et al. (2018). Human adult neurogenesis: evidence and remaining questions. Cell Stem Cell *23*, 25–30.

Leeman, D.S., Hebestreit, K., Ruetz, T., Webb, A.E., McKay, A., Pollina, E.A., Dulken, B.W., Zhao, X., Yeo, R.W., Ho, T.T., et al. (2018). Lysosome activation clears aggregates and enhances quiescent neural stem cell activation during aging. Science *359*, 1277–1283.

Llorens-Bobadilla, E., Zhao, S., Baser, A., Saiz-Castro, G., Zwadlo, K., and Martin-Villalba, A. (2015). Single-cell transcriptomics reveals a population of dormant neural stem cells that become activated upon brain injury. Cell Stem Cell *17*, 329–340.

Luo, J., Shook, B.A., Daniels, S.B., and Conover, J.C. (2008). Subventricular zone-mediated ependyma repair in the adult mammalian brain. J. Neurosci. *28*, 3804–3813.

Lupo, G., Gioia, R., Nisi, P.S., Biagioni, S., and Cacci, E. (2019). Molecular mechanisms of neurogenic aging in the adult mouse subventricular zone. J. Exp. Neurosci. *13*, 1179069519829040.

Lupo, G., Nisi, P.S., Esteve, P., Paul, Y.L., Novo, C.L., Sidders, B., Khan, M.A., Biagioni, S., Liu, H.K., Bovolenta, P., et al. (2018). Molecular

profiling of aged neural progenitors identifies Dbx2 as a candidate regulator of age-associated neurogenic decline. Aging Cell *17*, e12745.

Luque-Molina, I., Khatri, P., Schmidt-Edelkraut, U., Simeonova, I.K., Holzl-Wenig, G., Mandl, C., and Ciccolini, F. (2017). Bone morphogenetic protein promotes lewis X stage-specific embryonic antigen 1 expression thereby interfering with neural precursor and stem cell proliferation. Stem Cells *35*, 2417–2429.

Ma, P., Beck, S.L., Raab, R.W., McKown, R.L., Coffman, G.L., Utani, A., Chirico, W.J., Rapraeger, A.C., and Laurie, G.W. (2006). Heparanase deglycanation of syndecan-1 is required for binding of the epithelial-restricted prosecretory mitogen lacritin. J. Cell Biol. *174*, 1097–1106.

Maslov, A.Y., Barone, T.A., Plunkett, R.J., and Pruitt, S.C. (2004). Neural stem cell detection, characterization, and age-related changes in the subventricular zone of mice. J. Neurosci. *24*, 1726–1733.

Mich, J.K., Signer, R.A., Nakada, D., Pineda, A., Burgess, R.J., Vue, T.Y., Johnson, J.E., and Morrison, S.J. (2014). Prospective identification of functionally distinct stem cells and neurosphere-initiating cells in adult mouse forebrain. Elife *3*, e02669.

Morizur, L., Chicheportiche, A., Gauthier, L.R., Daynac, M., Boussin, F.D., and Mouthon, M.A. (2018). Distinct molecular signatures of quiescent and activated adult neural stem cells reveal specific interactions with their microenvironment. Stem Cell Rep. *11*, 565–577.

Obernier, K., and Alvarez-Buylla, A. (2019). Neural stem cells: origin, heterogeneity and regulation in the adult mammalian brain. Development *146*, dev156059.

Otsuki, L., and Brand, A.H. (2018). Cell cycle heterogeneity directs the timing of neural stem cell activation from quiescence. Science *360*, 99–102.

Pastrana, E., Silva-Vargas, V., and Doetsch, F. (2011). Eyes wide open: a critical review of sphere-formation as an assay for stem cells. Cell Stem Cell *8*, 486–498.

Pineda, J.R., Daynac, M., Chicheportiche, A., Cebrian-Silla, A., Sii Felice, K., Garcia-Verdugo, J.M., Boussin, F.D., and Mouthon, M.A. (2013). Vascular-derived TGF-beta increases in the stem cell niche and perturbs neurogenesis during aging and following irradiation in the adult mouse brain. EMBO Mol. Med. *5*, 548–562.

Roccio, M., Schmitter, D., Knobloch, M., Okawa, Y., Sage, D., and Lutolf, M.P. (2013). Predicting stem cell fate changes by differential cell cycle progression patterns. Development *140*, 459–470.

Sakaue-Sawano, A., Kurokawa, H., Morimura, T., Hanyu, A., Hama, H., Osawa, H., Kashiwagi, S., Fukami, K., Miyata, T., Miyoshi, H., et al. (2008). Visualizing spatiotemporal dynamics of multicellular cell-cycle progression. Cell *132*, 487–498.

Salomoni, P., and Calegari, F. (2010). Cell cycle control of mammalian neural stem cells: putting a speed limit on G1. Trends Cell Biol. *20*, 233–243.

Sanai, N., Nguyen, T., Ihrie, R.A., Mirzadeh, Z., Tsai, H.H., Wong, M., Gupta, N., Berger, M.S., Huang, E., Garcia-Verdugo, J.M., et al. (2011). Corridors of migrating neurons in the human brain and their decline during infancy. Nature *478*, 382–386.

Shook, B.A., Manz, D.H., Peters, J.J., Kang, S., and Conover, J.C. (2012). Spatiotemporal changes to the subventricular zone stem cell pool through aging. J. Neurosci. *32*, 6947–6956.

Silva-Vargas, V., Maldonado-Soto, A.R., Mizrak, D., Codega, P., and Doetsch, F. (2016). Age-Dependent niche signals from the choroid plexus regulate adult neural stem cells. Cell Stem Cell *19*, 643–652.

Tropepe, V., Craig, C.G., Morshead, C.M., and van der Kooy, D. (1997). Transforming growth factor-alpha null and senescent mice show decreased neural progenitor cell proliferation in the forebrain subependyma. J. Neurosci. *17*, 7850–7859.

Wang, Q., Yang, L., Alexander, C., and Temple, S. (2012). The niche factor syndecan-1 regulates the maintenance and proliferation of neural progenitor cells during mammalian cortical development. PLoS One *7*, e42883.

iScience, Volume *23*

Supplemental Information

Syndecan-1 Stimulates Adult Neurogenesis in the Mouse Ventricular-Subventricular Zone after Injury

Marc-André Mouthon, Lise Morizur, Léa Dutour, Donovan Pineau, Thierry Kortulewski, and François D. Boussin

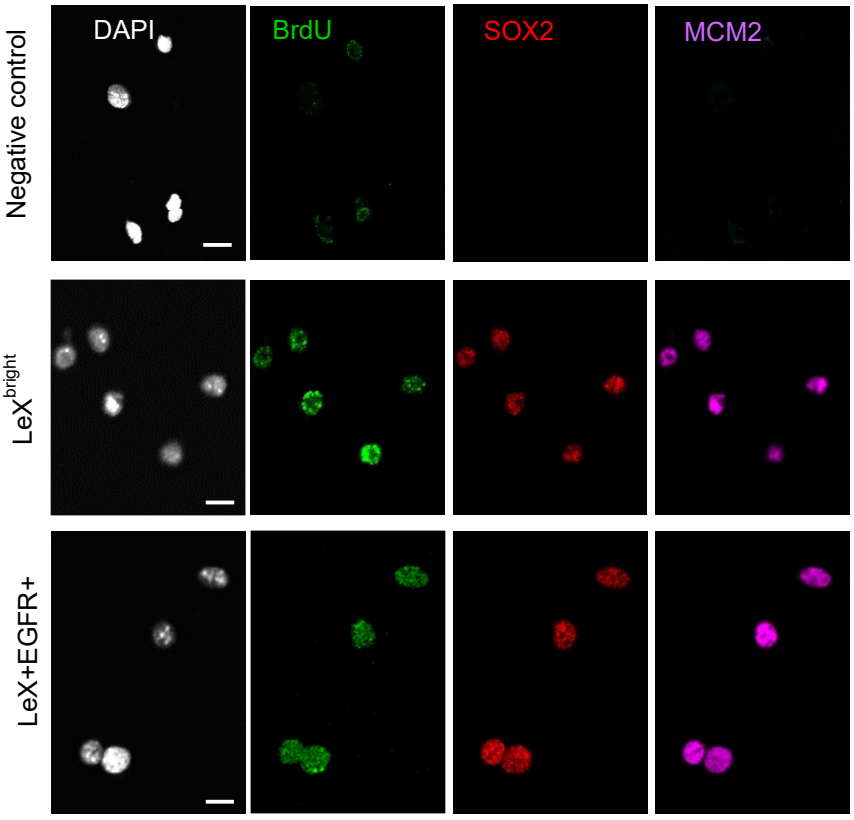
DAPI
BrdU
SOX2
MCM2
Negative control
LeX^bright
LeX+EGFR+

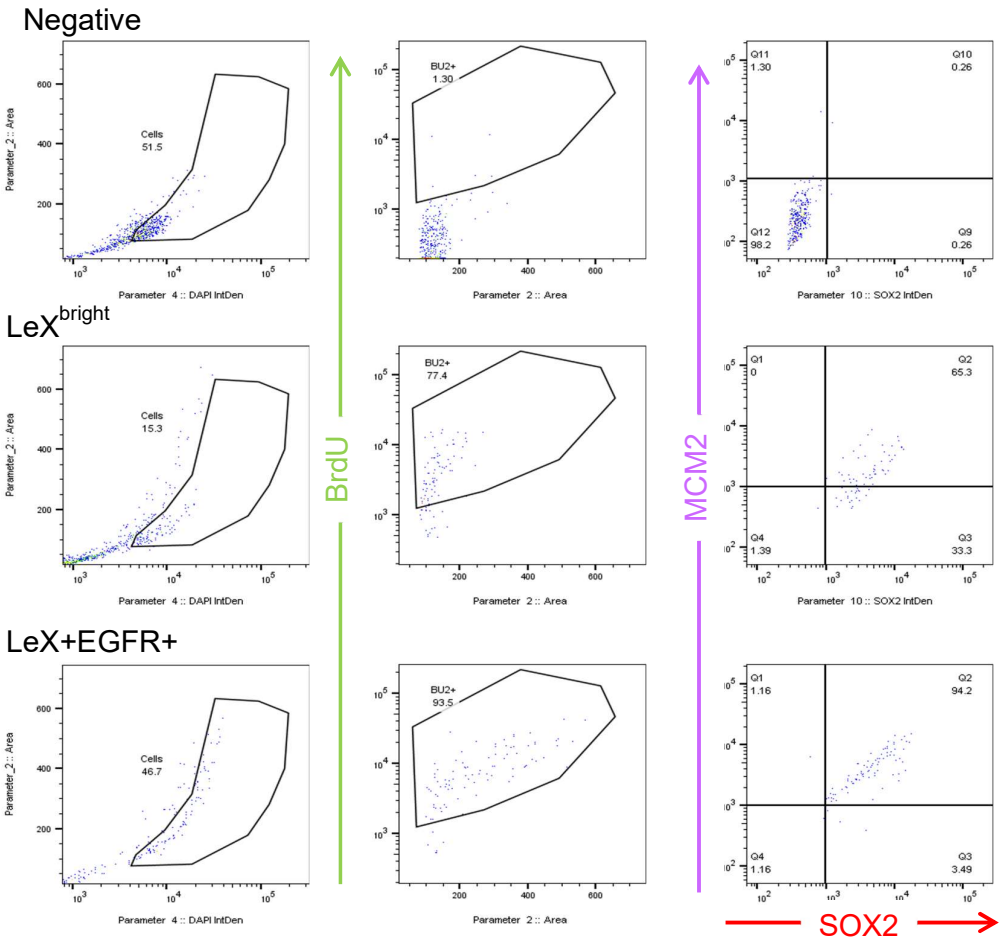
Negative
LeX^bright
LeX+EGFR+
Cells
51.5
Cells
15.3
Cells
46.7
BU2+
1.30
BU2+
77.4
BU2+
93.5
Q11
1.30
Q10
0.26
Q12
98.2
Q9
0.26
Q1
0
Q2
65.3
Q4
1.39
Q3
33.3
Q1
1.16
Q2
94.2
Q4
1.16
Q3
3.49
Parameter 4 :: DAPI IntDen
Parameter 2 :: Area
Parameter 10 :: SOX2 IntDen
Parameter_2 :: Area
BrdU
MCM2
SOX2

Figure S1

Figure S1: Young adult LeX^{bright} qNSCs are produced during embryogenesis, Related to Figure1.

(A) Representative pictures of BrdU/SOX2/MCM2 immunostaining in LeXbright and LeX+EGFR+ are shown. (B) Quantification of BrdU/SOX2/MCM2 immunostaining in LeXbright and LeX+EGFR+ sorted cells with FlowJo. Scale bars = 10 μm.

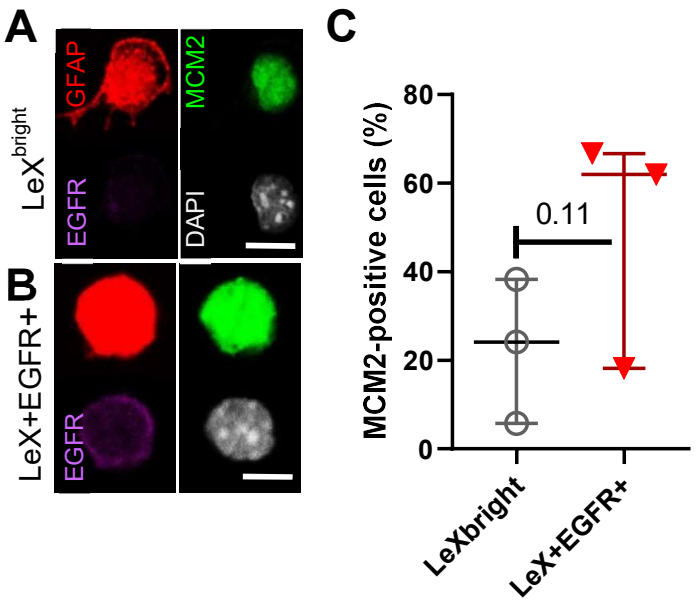
A
LeX^bright
GFAP
EGFR
MCM2
DAPI
B
LeX+EGFR+
EGFR
C
MCM2-positive cells (%)
80
60
40
20
0
0.11
LeXbright
LeX+EGFR+

Figure S2

Figure S2: Early postnatal LeX^{bright} qNSCs are primed to enter cell cycle, Related to Figure 1.

(A) LeX^{bright} qNSCs and (B) LeX+EGFR+ aNSCs were sorted from neonatal brains (10 days) and the expressions of GFAP (red) and MCM2 (green) were examined (Scale bars = 10 μm). (B) The presence of EGFR is shown at the membrane of aNSCs. (C) Quantifications of MCM2 are represented as median ± interquartile of replicate experiments.

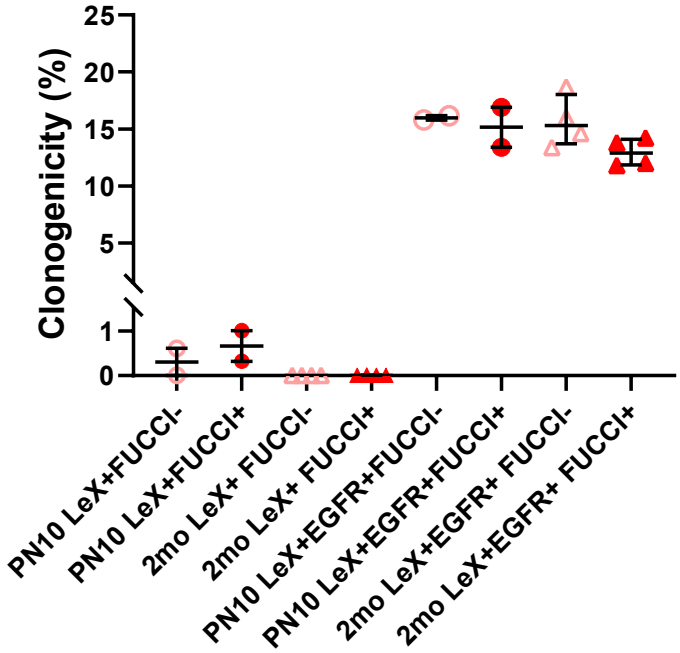
Clonogenicity (%)
25
20
15
10
5
1
0
PN10 LeX+FUCCI-
PN10 LeX+FUCCI+
2mo LeX+ FUCCI-
2mo LeX+ FUCCI+
PN10 LeX+EGFR+FUCCI-
PN10 LeX+EGFR+FUCCI+
2mo LeX+EGFR+ FUCCI-
2mo LeX+EGFR+ FUCCI+

Figure S3

Figure S3: Formation of neurospheres with LeX^{bright} and LeX+EGFR+ cells sorted from V-SVZ at different ages according to FUCCI fluorescence, Related to Figure 2.

The formation of neurospheres was determined for LeX^{bright} qNSCs and LeX+EGFR+ aNSCs accordingly to their FUCCI fluorescence (FUCCI^{neg} S/G_2/M and FUCCI^{pos} G_1) obtained from 10 days-neonates and 2 months-old mice. Data are represented as median ± interquartile. Each dot represents individual experiment with 3 to 4 mice. Consistently with their exit from the cell cycle, FUCCI^{bright} G_0 cells did not gave rise to neurospheres (data not shown).

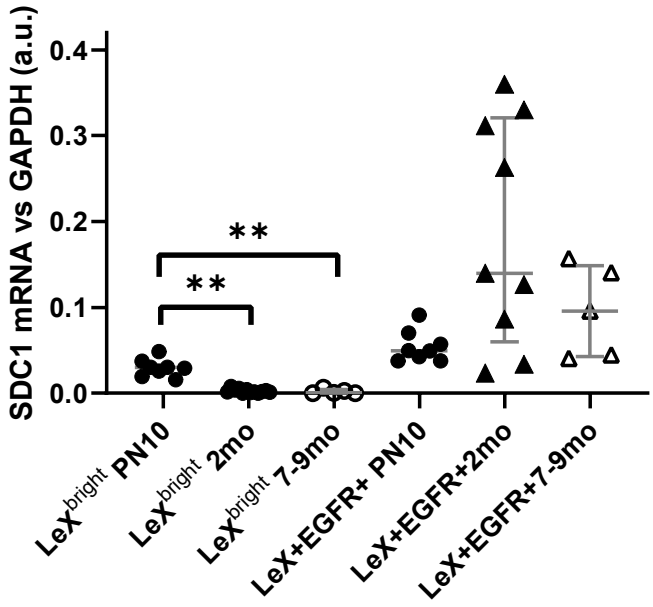
SDC1 mRNA vs GAPDH (a.u.)
0.4
0.3
0.2
0.1
0.0
**
**
LeX^bright PN10
LeX^bright 2mo
LeX^bright 7-9mo
LeX+EGFR+ PN10
LeX+EGFR+2mo
LeX+EGFR+7-9mo

Figure S4

Figure S4: SDC1 mRNA expression in qNSCs and aNSCs with aging, Related to Figure 4.

LeX^{bright} qNSCs and LeX+EGFR+ aNSCs were sorted from neonates (PN10), young adults (2 months) and mid-aged (7-9 months-old) V-SVZ, then SDC1 mRNA expression level was quantified by qRT-PCR as previously reported (Morizur et al., 2018).

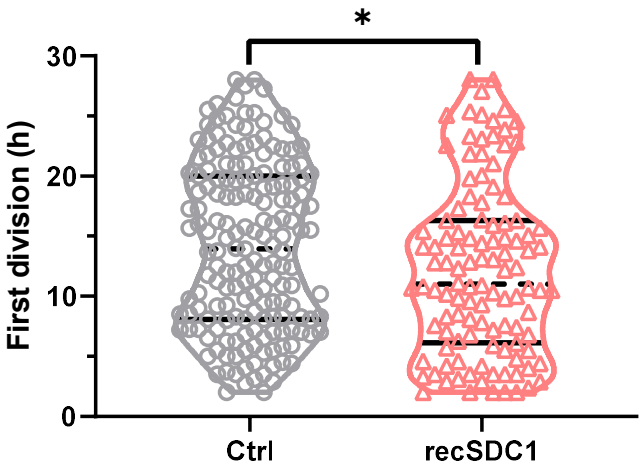

Figure S5

Figure S5: Exogenous SDC1 hastens division of LeX+EGFR+ aNSCs from adult V-SVZ, Related to Figure 4.

LeX+EGFR+ aNSCs were sorted from young adult V-SVZ and followed by timelapse for 26-30h in the absence, or the presence, of 2.5µg/ml recSDC1. The time for the first division was recorded. Each dot represents a single division. Data are represented as the median ± interquartile range of 4 replicate experiments with 3 to 4 mice per group.

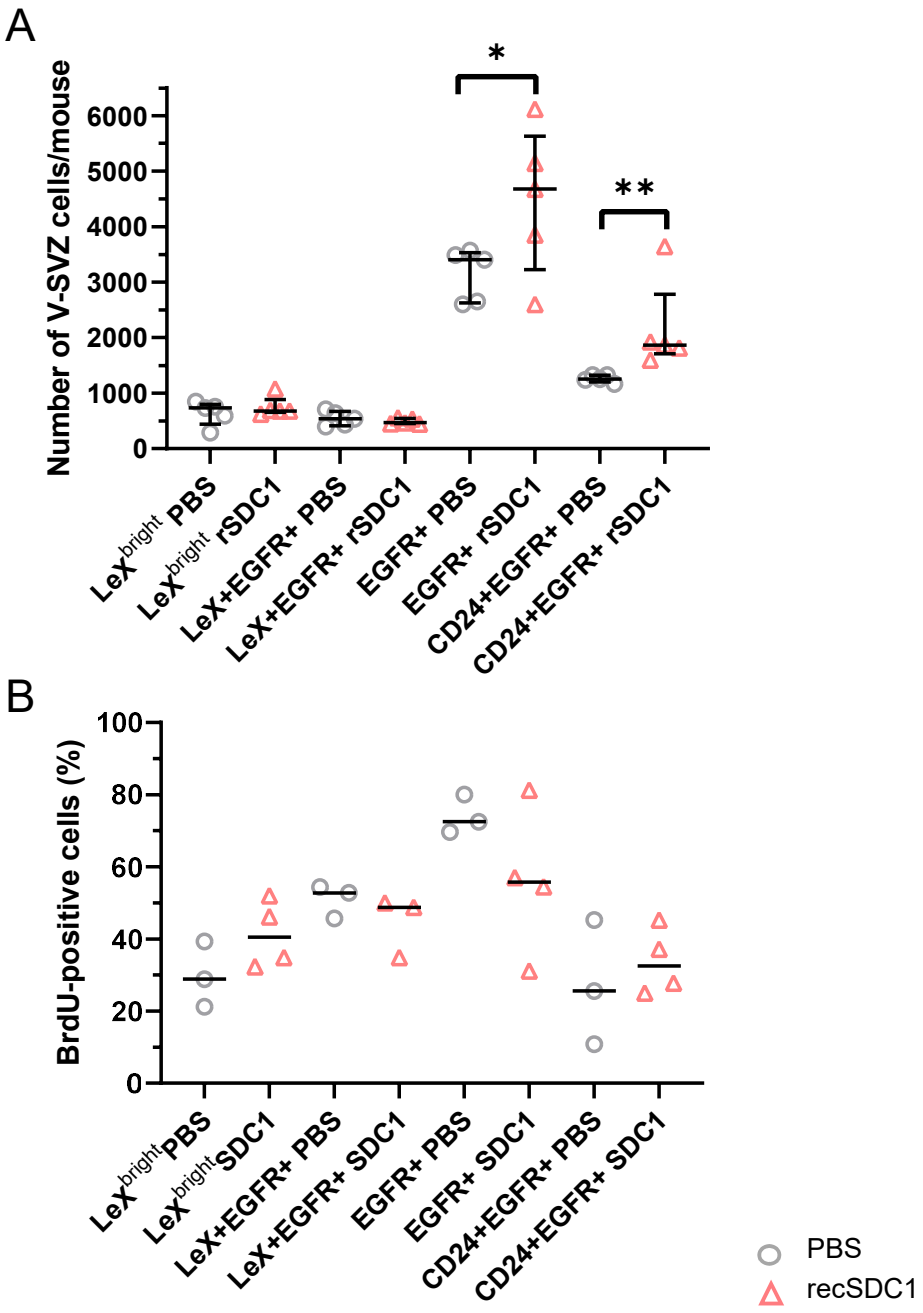
A
Number of V-SVZ cells/mouse
6000
5000
4000
3000
2000
1000
0
*
**
LeX^bright PBS
LeX^bright rSDC1
LeX+EGFR+ PBS
LeX+EGFR+ rSDC1
EGFR+ PBS
EGFR+ rSDC1
CD24+EGFR+ PBS
CD24+EGFR+ rSDC1
B
BrdU-positive cells (%)
100
80
60
40
20
0
LeX^brightPBS
LeX^brightSDC1
LeX+EGFR+ PBS
LeX+EGFR+ SDC1
EGFR+ PBS
EGFR+ SDC1
CD24+EGFR+ PBS
CD24+EGFR+ SDC1
PBS
recSDC1

Figure S6

Figure S6: Exogenous SDC1 administration ameliorates recovery of neurogenic populations after V-SVZ injury, Related to Figure 5.

Two-months-old adult FUCCI-Cdt1 mice were irradiated (4 Gy/head only) and received recSDC1 intraventricularly. (A) The absolute numbers of LeX^{bright} qNSCs, LeX+EGFR+ aNSCs, EGFR+ progenitors and CD24+EGFR+ proliferating neuroblasts were determined by flow cytometry. Each plot represents an individual mouse. (B) The different neurogenic populations were sorted and BrdU incorporation was examined by immunofluorescence. For several mice, sorted cells have been pooled to determine the BrdU incorporation. Data are represented as median ± interquartile range. Data obtained from SDC1-treated groups were compared to PBS-treated groups using non-parametric Mann-Whitney test. A significant difference was obtained only for the total number of EGFR and CD24+EGFR+ cells/mouse: $P<0.05$ (*) and <0.005 (**).

Table S1: Kruskal-Wallis and Dunn's multiple comparison analyses of FUCCI content in LeX+EGFR+ and LeX^{bright} NSCs, Related to Figure 2A-B.

	LeX^{bright}						LeX+EGFR+				
Age	PN4	PN9	PN10	2 mo	12 mo		PN4	PN9	PN10	2 mo	12 mo
PN4				*	*					°*	°*
PN9				***	**					*	**
PN10				****	**						*
2 mo											
n=	3	4	20	27	6		3	4	20	27	6

°: FUCCI^{high} (G0) and *: FUCCI^{neg} (S/G2/M).
n = indicates the number of mice per group.

Table S2: List of genes from GEO Data Set GSE99777 (Morizur et al., 2018) belonging to WNT signaling pathway and increased in LeX^{bright} qNSCs after V-SVZ radio-induced injury, related to Figure 5.

Gene symbol	Gene ID
Apc2	23805
Arid1a	93760
Csnk2a2	13000
Ep300	328572
Gnaq	14682

Gene symbol	Gene ID
Nkd1	93960
Pcdh1	75599
Pcdh8	18530
Pcdh9	211712

Gene symbol	Gene ID
Ppp3cb	19056
Smarcal1	54380
Tcf3	21415
Wdr61	66317

TRANSPARENT METHODS

Animals and treatments

FUCCI-Cdt1 transgenic mice (fluorescence ubiquitination-based cell cycle indicator) (Sakaue-Sawano et al., 2008) and C57Bl/6J mice were maintained in standard cages with access to food and water ad libitum in a colony room kept at a constant temperature (19-22°C) and humidity (40-50%) on a 12:12-hour light/dark cycle. Pregnant mice and early postnatal pups were produced in our animal facility by programmed breeding.

Pregnant mice were injected intraperitoneally with BrdU 100 mg/kg body mass 3 time/day for two days (E14.5 to E15.5).

When indicated, young adult (2-3 months-old) mice received whole brain irradiation (4 Gy) under anesthesia using a ^{60}Co medical irradiator (Alcyon) or a Small Animal Radiation Research Platform (SARRP; Xstrahl) as previously reported (Daynac et al., 2013).

For *in vivo* SDC1 treatment, FUCCI mice received intraventricularly 5µg of recombinant murine SDC1 (R&D) through strereotaxia (AP-0.1; ML+0.1; V-2.5) two days after brain irradiation. BrdU (100 mg/kg) was injected intraperitoneally 4-6h after stereotaxia then BrdU was given in the drinking water (1 mg/ml) until sacrifice three days later.

Animal experiments were performed in compliance with the European Communities Council Directive of 22th September 2010 (EC/2010/63) and were approved by our institutional committee on animal welfare (CEtEA-CEA DRF IdF) and registrated at the French Ministry of Education and Research (APAFIS#2723-2015111710123712).

V-SVZ cell preparation and FACS sorting/analysis

Mouse V-SVZs were dissected from early postnatal and adult brains then dissociated and labelled as previously described (Daynac et al., 2013; Daynac et al., 2015; Morizur et al., 2018). V-SVZ were minced then mechanichally dissociated and for adult brains after a preliminary 10-min digestion step with papain (1 mg/ml, Worthington). Remaining aggregates were removed with 20 µm nylon filters (BD Biosciences) and cells were centrifuged at 250 g for 20 min on a 22% Percoll gradient (GE Healthcare). Then, cells were incubated for 20 min with the following antibodies: CD24 phycoerythrin [PE]-conjugated (cat#561079; 1:100 BD Biosciences), or anti-CD24 PE-Cyanine7-conjugated (cat#A14776, 1:100 Molecular Probes), CD15/LeX fluorescein isothiocyanate [FITC]-conjugated (clone MMA, mouse IgM; 1:50 BD Biosciences) and Alexa647-conjugated EGF ligand (1:250 Life Technologies). V-SVZ cells were sorted on an INFLUX cell sorter equipped with an 86 µm nozzle at 40 psi or on an ARIA II equipped with a 100 µm nozzle (BD Biosciences). In some experiments, the absolute number of cells was normalized using Trucount beads (BD Biosciences). Gates were set using Fluorescence Minus One (FMO) controls on V-SVZ cells. qNSCs were collected in $CD24^{low}EGFR^{neg}LeX^{bright}$ (hereafter noted LeX^{bright}) and aNSCs were collected in $CD24^{low}EGFR^{pos}LeX^{pos}$ (hereafter noted LeX+EGFR+). The FUCCI-Cdt1 red fluorescence was captured into the PE channel and three populations were collected according to red fluorescence intensity, i.e. $FUCCI^{neg}$, $FUCCI^{pos}$ and $FUCCI^{high}$ (Daynac et al., 2014).

Cell culture

Sorted NSCs were grown at 37°C 5% CO2 in enriched NSC medium (Codega et al., 2014) composed of DMEM/F12 (Life Technologies) supplemented with 0.6% Glucose (Sigma), 2µg/mL heparin (STEMCELL Technologies), 1x Insulin-Selenium-Transferrin (Life Technologies), N-2 supplement (Life Technologies) and B-27 without Vitamin A supplement (Life Technologies), and in the presence of 20 ng/ml EGF (Millipore) and 10 ng/ml FGF2 (Millipore). In some experiments, 2.5 µg/ml of recombinant mouse SDC1 (R&D Systems) was added to the medium. Sorted cells were plated at a density not exceeding 1.4 cells/µl in 12 or 24 well plates which were leaved untouched until neurosphere counting. After 6-7 days, neurospheres were counted under an inverted microscope.

Live Cell Imaging

Freshly sorted cells were plated in NSC medium described above on laminin (Biolaminin521-coated slides (Biolamina) coated glass-bottomed culture plates (MatTek, Corp., Ashland, MA). Brightfield and fluorescent images for Cdt1-red were captured through a Plan Apo VC ×20 DIC objective (NA: 0.75) on a Nikon A1R confocal laser scanning microscope system attached to an inverted ECLIPSE Ti (Nikon, Corp., Tokyo, Japan) thermostated at 37°C under 5% of CO2 and 18% of O_2 atmosphere (Daynac et al., 2014). Live imaging started 2-3 hours after plating. Single-cell tracking was performed over periods of up to 24 hours with images taken at 15 minutes intervals in order to follow the fate of individual cells. Images and time-lapse videos were analyzed with ImageJ and NIS-Elements (Nikon) softwares.

Immunofluorescence

Sorted cells were recovered in NSC medium then plated without mitogen on Biolaminin521-coated slides (Biolamina) in an incubator at 37°C 5% CO2 for 4 hours and fixed in 2% paraformaldehyde. After 1 hour in blocking solution (PBS-0.1% Triton-X100, 0.05% Tween 20, 4% BSA) at RT, cells were incubated overnight at 4°C with primary antibodies: goat anti-MCM2 (1:300; Santa Cruz) or rabbit anti-MCM2 (1:400; Novus), goat anti-SOX2 (1:20; R&D), rabbit anti-phospho-S6 ribosomal protein (Ser240/244) 1:1000; CellSignaling). For BrdU detection, mild DNA digestion was performed for 30 min at 37°C in DNase (10 µg/mL DNase I, 0.5x PBS, 30 mM Tris-HCl pH 8, 0.3 mM MgCl2, 0.5 mM 2-mercaptoethanol, 0.5% BSA) then incubated with anti-BrdU antibody at 1:300 (GE Healthcare). After overnight incubation with primary antibodies at 4°C, three washes in PBS, cells were incubated with AlexaFluor 488/594/647 goat/donkey cross-species absorbed secondary antibodies at 1:800 (Invitrogen).

Immunofluorescence analyses

Immunostaining in 96-well plates were imaged using a Nikon A1R confocal microscope. Image analyses were performed using ImageJ. Region Of Interest were drawn on DAPI staining and multiple immunoflorescences were measured within the nuclus masks. CSV files were converted into FCS format then analysed with FlowJo v10.7.1.

Statistical analyses

The data are expressed as the median with interquartile range. Non-parametric two-tailed Mann-Whitney, Kruskal-Wallis and Dunn's multiple comparison tests were conducted to compare data using GraphPad PRISM software (GraphPad, San Diego, CA). P-value levels were set at <0.05 (*), <0.005 (**), <0.0005 (***) and <0.00005 (****).

SUPPLEMENTAL REFERENCES

Codega, P., Silva-Vargas, V., Paul, A., Maldonado-Soto, A. R., Deleo, A. M., Pastrana, E., and Doetsch, F. (2014). Prospective identification and purification of quiescent adult neural stem cells from their in vivo niche. Neuron *82*, 545-559.

Daynac, M., Chicheportiche, A., Pineda, J. R., Gauthier, L. R., Boussin, F. D., and Mouthon, M. A. (2013). Quiescent neural stem cells exit dormancy upon alteration of GABAAR signaling following radiation damage. Stem Cell Res *11*, 516-528.

Daynac, M., Morizur, L., Kortulewski, T., Gauthier, L. R., Ruat, M., Mouthon, M. A., and Boussin, F. D. (2015). Cell Sorting of Neural Stem and Progenitor Cells from the Adult Mouse Subventricular Zone and Live-imaging of their Cell Cycle Dynamics. J Vis Exp.

Daynac, M., Pineda, J. R., Chicheportiche, A., Gauthier, L. R., Morizur, L., Boussin, F. D., and Mouthon, M. A. (2014). TGFbeta lengthens the G1 phase of stem cells in aged mouse brain. Stem Cells *32*, 3257-3265.
Morizur, L., Chicheportiche, A., Gauthier, L. R., Daynac, M., Boussin, F. D., and Mouthon, M. A. (2018). Distinct Molecular Signatures of Quiescent and Activated Adult Neural Stem Cells Reveal Specific Interactions with Their Microenvironment. Stem Cell Reports *11*, 565-577.
Sakaue-Sawano, A., Kurokawa, H., Morimura, T., Hanyu, A., Hama, H., Osawa, H., Kashiwagi, S., Fukami, K., Miyata, T., Miyoshi, H.*, et al.* (2008). Visualizing spatiotemporal dynamics of multicellular cell-cycle progression. Cell *132*, 487-498.